



Stability and Thermoelasticity of Diaspore by Synchrotron X-ray Diffraction and Raman Spectroscopy

Shijie Huang^{1,2}, Jingui Xu³, Daorong Liu⁴, Bo Li^{1,2}, Zhilin Ye^{1,2}, Wei Chen^{1,2,5}, Yunqian Kuang^{1,2,6}, Fangli Chi⁷, Dawei Fan^{1*}, Maining Ma^{8*} and Wenge Zhou¹

¹Key Laboratory of High-Temperature and High-Pressure Laboratory for High Temperature and High Pressure Study of the Earth's Interior, Institute of Geochemistry, Chinese Academy of Sciences, Guiyang, China, ²University of Chinese Academy of Sciences, Beijing, China, ³Hawai'i Institute of Geophysics and Planetology, School of Ocean and Earth Science and Technology, University of Hawai'i at Manoa, Honolulu, HI, United States, ⁴Zhejiang Geological Prospecting Institute of China Chemical Geology and Mine Bureau, Hangzhou, China, ⁵Guizhou Polytechnic of Construction, Guiyang, China, ⁶Bureau of Natural Resources and Planning of Yongzhou, Yongzhou, China, ⁷Key Laboratory of Urban Sewage Treatment of Jilin Province, Changchun Institute of Technology, Changchun, China, ⁸Key Laboratory of Computational Geodynamics, College of Earth and Planetary Sciences, University of Chinese Academy of Sciences, Beijing, China

OPEN ACCESS

Edited by:

Hongzhan Fei,
University of Bayreuth, Germany

Reviewed by:

Yu Ye,
China University of Geosciences
Wuhan, China
Wen-Yi Zhou,
University of New Mexico,
United States

*Correspondence:

Dawei Fan
fandawei@vip.gyig.ac.cn
Maining Ma
mamn@ucas.ac.cn

Specialty section:

This article was submitted to
Earth and Planetary Materials,
a section of the journal
Frontiers in Earth Science

Received: 03 August 2021

Accepted: 02 September 2021

Published: 24 September 2021

Citation:

Huang S, Xu J, Liu D, Li B, Ye Z,
Chen W, Kuang Y, Chi F, Fan D, Ma M
and Zhou W (2021) Stability and
Thermoelasticity of Diaspore by
Synchrotron X-ray Diffraction and
Raman Spectroscopy.
Front. Earth Sci. 9:752566.
doi: 10.3389/feart.2021.752566

The thermoelasticity and stability of diaspore (α -AlOOH, $\text{Al}_{1.002}\text{Fe}_{0.003}\text{OOH}$) were investigated in this study by *in situ* synchronous X-ray diffraction (XRD) and Raman spectroscopy methods at high pressure and high temperature conditions. The results indicate that diaspore is stable within the pressure and temperature (P - T) region examined in this study. With increasing pressure, the Raman peaks move toward the high wave number direction, the intensity of the Raman peaks increases, and the vibration mode of diaspore changes linearly. Pressure-volume data from *in situ* high-pressure XRD experiments were fitted by the third-order Birch-Murnaghan equation of state (EoS) with the zero-pressure unit-cell volume $V_0 = 118.15$ (4) \AA^3 , the zero-pressure bulk modulus $K_{V0} = 153$ (2) GPa, and its pressure derivative $K'_{V0} = 2.4$ (3). When K'_{V0} was fixed at 4, the obtained $K_{V0} = 143$ (1) GPa. The axial compressional behavior of diaspore was also fitted with a linearized third-order Birch-Murnaghan EoS, showing slight compression anisotropy with $K_{a0} = 137$ (5) GPa, $K_{b0} = 169$ (7) GPa and $K_{c0} = 178$ (6) GPa. In addition, the temperature-volume data from *in situ* high-temperature XRD experiments were fitted by Fei's thermal equation with the thermal expansion coefficients $\alpha_V = 2.7$ (2) $\times 10^{-5} \text{ K}^{-1}$, $\alpha_a = 1.13$ (9) $\times 10^{-5} \text{ K}^{-1}$, $\alpha_b = 0.77$ (5) $\times 10^{-5} \text{ K}^{-1}$, and $\alpha_c = 0.85$ (9) $\times 10^{-5} \text{ K}^{-1}$ for diaspore, which shows that diaspore exhibits slightly anisotropic thermal expansion. Furthermore, *in situ* synchrotron-based single-crystal XRD under simultaneously high P - T conditions indicates that the P - T stability of diaspore is up to ~ 10.9 GPa and 700 K. Combined with previous results, we infer that diaspore can be subducted to ~ 390 km under cold subduction conditions based on existing experimental data and is a good candidate for transporting water to the deep Earth.

Keywords: diaspore, high pressure and high temperature, diamond anvil cell, synchrotron X-ray diffraction, Raman spectroscopy

INTRODUCTION

Subduction zones are the bridge between the Earth's surface and the deep Earth (Hwang et al., 2021). Subduction transports crustal hydration minerals to the mantle, and the hydrous minerals in the subduction zone under the volcanic arc are often dehydrated under the temperature and pressure of the mantle, which leads to the generation of island arc magma (Zheng and Zhao, 2017). This process plays an important role in the water cycle of the deep Earth. In addition, the migration of water to the mantle has important geodynamic and geochemical significance. The dehydration of hydrous minerals in the mantle hydrates nominally anhydrous minerals there and affects the viscosity and density structure of the mantle (Hebert and Montesi, 2013). Moreover, dehydration of hydrous minerals also leads to the brittle fracture of plates, triggering medium-depth earthquakes (Zheng, 2019). Therefore, the structural stability and thermoelastic properties of hydrous minerals under high-pressure and high-temperature (high P - T) conditions are often regarded as a window through which to study the geodynamic process of the deep Earth (Nakao et al., 2016; Kakizawa et al., 2018; Liu et al., 2019; Zhang et al., 2019; Liu et al., 2021).

During the subduction process, the water-rich fluids react with the gneiss or metamorphic argillaceous rocks of the subducted continental crust along the wet solid phase line to form water-rich melts, which are granitic components and the main source of magmatic material in island arcs (Zheng, 2019). In addition, the Al-rich hydrous silicate minerals in the subduction zone can transport not only water but also Al to the deep mantle, and the

entry of Al as a crustal element into the mantle will affect the composition of the mantle (Tropper and Manning, 2007). Diaspore (α -AlOOH), which contains 28.3 wt% water and has a wide range of temperature and pressure stabilities (Mao et al., 1994; Sugiura et al., 2018), is an important Al-rich hydrous mineral in subduction zones (Vanpeteghem et al., 2002; Sano et al., 2008; Wang and Yoshino, 2021). During the eclogite lithification of bauxite, diaspore decomposes into corundum at approximately 1073 K under 7 GPa and releases 6–8 wt% water (Grevel et al., 2000; Feenstra and Wunder, 2002). However, under cold subduction conditions, diaspore transforms to a high-pressure phase (δ -AlOOH) and continue to subduct to the core-mantle boundary (Sano et al., 2008). Therefore, the study about the thermal equation of state (EoS) and the high P - T stability of diaspore is of great significance for understanding the migration of Al and water in the deep Earth, especially in subduction zones.

The symmetry of diaspore is orthorhombic $Pbnm$. In the crystal structure of diaspore (Figure 1) (Hill, 1979), Al³⁺ occupies the center of the octahedron position, and the O atom is closely packed hexagonally along the a -axis. Adjacent [AlO₆] octahedrons share four sides, forming “double rutile strings” parallel to the c -axis and connected with each other through corner sharing (Ewing, 1935; Friedrich et al., 2007a). There are two types of O atoms: O1 with corner sharing and O2 with edge sharing. H is chemically bonded to O2 and forms a hydrogen bond with O1.

The pressure-volume (P - V) EoS of diaspore has been studied experimentally and theoretically (Table 1) (Mao et al., 1994; Xu et al., 1994; Winkler et al., 2001; Friedrich et al., 2007a, 2007b; Li

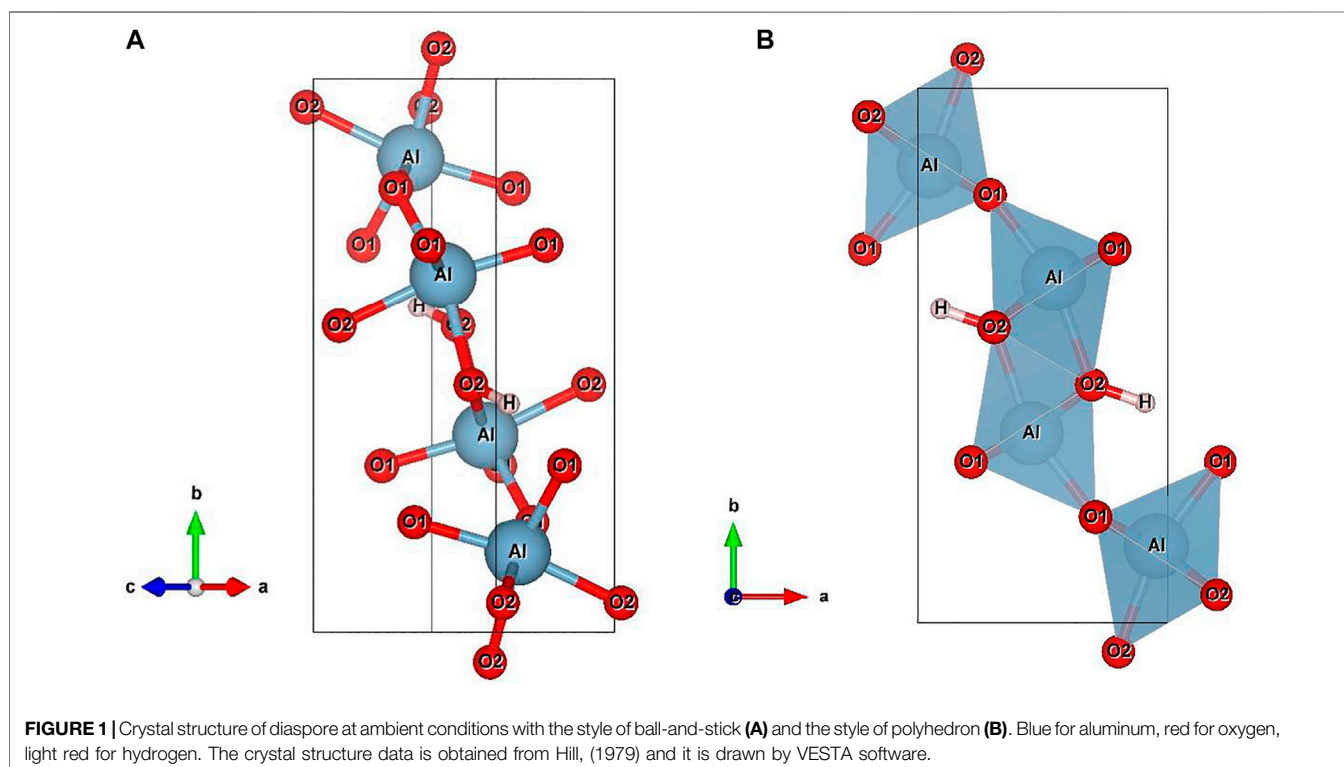


TABLE 1 | Elastic parameters of diaspore.

Samples	P (GPa)	T (K)	K_{V0} (GPa)	K'_{V0}	K_{SV}	K_{a0} (GPa)	K'_{a0}	K_{b0} (GPa)	K'_{b0}	K_{c0} (GPa)	K'_{c0}	Methods	Pressure medium	References
AlO(OH)	—	—	145.3 (4)	—	150.7 (3)	—	—	—	—	—	—	UE ^a	—	Haussuhl (1993)
—	24.54	300	168 (2)	4 (fixed)	—	92 (5)	4 (fixed)	225 (6)	4 (fixed)	221 (21)	4 (fixed)	P-XRD ^b	methanol-ethanol (4:1)	Mao et al. (1994)
—	24.54	300	170 (14)	3 (1)	—	133 (12)	3 (2)	202 (21)	6 (2)	223 (56)	11(15)	P-XRD ^b	methanol-ethanol (4:1)	Mao et al. (1994)
AlO(OH)	27	300	227 (5)	4	—	136 (9)	4	136 (9)	4	260 (22)	4	XRD	no pressure medium	Xu et al. (1994)
AlO(OH)	50	300	147 (2)	4.5 (1)	—	—	—	—	—	—	—	DFT ^c	—	Winkler et al. (2001)
AlO(OH)	50	300	151 (2)	4 (fixed)	—	104 (2)	4 (fixed)	180 (6)	6 (fixed)	184 (3)	3.44 (fixed)	SC-XRD ^d	Helium	Friedrich et al. (2007a)
AlO(OH)	50	300	149 (4)	4.1 (2)	—	102 (2)	4.2 (2)	194 (16)	5 (1)	189 (11)	3.2 (5)	SC-XRD ^d	Helium	Friedrich et al. (2007a)
AlO(OH)	50	300	150.4 (9)	4 (fixed)	—	—	—	—	—	—	—	DFT ^c	—	Friedrich et al. (2007a)
AlO(OH)	50	300	143.7 (9)	4.44 (6)	—	107.8 (7)	4.14 (5)	166 (2)	6.1 (1)	174.2 (5)	3.44 (2)	DFT ^c	—	Friedrich et al. (2007a)
AlO(OH)	7	300	150 (3)	4 (fixed)	—	103 (2)	4 (fixed)	191 (14)	6 (fixed)	188 (9)	3.44 (fixed)	SC-XRD ^d	methanol-ethanol (4:1)	Friedrich et al. (2007b)
AlO(OH)	40	300	150.4 (9)	4 (fixed)	—	—	—	—	—	—	—	DFT ^c	—	Friedrich et al. (2007b)
AlO(OH)	40	300	143.7 (9)	4.44 (6)	—	107.8 (7)	4.14 (5)	166 (2)	6.1 (1)	174.2 (5)	3.44 (2)	DFT ^c	—	Friedrich et al. (2007b)
(Al _{0.995} Fe _{0.005}) OOH	12	300	146 (1)	4.0 (1)	152 (1)	—	—	—	—	—	—	BS ^e	methanol-ethanol-water (16:3:1)	Jiang et al. (2008)
Al _{1.002} Fe _{0.003} OOH	13.42	300	143 (1)	4	—	137 (5)	4	169 (7)	4	178 (6)	4	SC-XRD ^d	Neon	This study
Al _{1.002} Fe _{0.003} OOH	13.42	300	153 (2)	2.4 (3)	—	—	—	—	—	—	—	SC-XRD ^d	Neon	This study

—, No data.

^aUltrasonic elasticity.^bPolycrystalline X-ray diffraction.^cDensity functional theory.^dSingle-crystal X-ray diffraction.^eBrillouin scattering.

et al., 2008). However, the previous P - V EoS results for diaspore are controversial. Xu et al. (1994) investigated the high-pressure behavior of diaspore using *in situ* synchrotron X-ray diffraction (XRD) up to ~ 27 GPa with no pressure medium and obtained a zero-pressure bulk modulus $K_{V0} = 227$ (5) GPa, and its pressure derivative (K'_{V0}) was set to 4. Mao et al. (1994) also investigated the compressibility of diaspore up to 24.51 GPa with a methanol-ethanol (4:1) pressure medium by *in situ* synchrotron polycrystalline XRD and obtained $K_{V0} = 168$ (2) GPa, which is $\sim 26\%$ lower than that of Xu et al. (1994). Subsequently, using an *in situ* synchrotron single-crystal XRD method, Friedrich et al. (2007a, and 2007b) investigated the P - V EoS of diaspore with two different pressure media (helium and methanol-ethanol (4:1)) up to ~ 50 and ~ 7 GPa, respectively, and obtained very consistent results for the bulk modulus ($K_{V0} = 151$ (2) GPa and 150 (3) GPa, respectively). However, the obtained bulk moduli of diaspore by Friedrich et al. (2007b) are still $\sim 11\%$ lower than those of Mao et al. (1994). Additionally, Jiang et al. (2008) further studied the elastic properties of diaspore by the Brillouin light-scattering method up to 12 GPa with methanol-ethanol-water (16:3:1) pressure medium and obtained the adiabatic zero-pressure bulk modulus $K_{S0} = 152$ (1) ($K_{V0} = 146$ (1) GPa), which is relatively consistent with that of Friedrich et al. (2007b) but $\sim 13\%$ lower than that of Mao et al. (1994) within their uncertainties (Mao et al., 1994; Friedrich et al., 2007b; Jiang et al., 2008). On the other hand, there are also some theoretical calculation studies on the P - V EoS of diaspore. Winkler et al. (2001) and Friedrich et al. (2007a) studied the P - V EoS of diaspore up to 50 GPa using the density functional theory method and obtained $K_{V0} = 147$ (2) GPa and 143.7 (9) GPa and $K'_{V0} = 4.5$ (1) and 4.44 (6), respectively (Winkler et al., 2001). However, the K'_{V0} of Friedrich et al. (2007a) is 8.8% lower than that of Winkler et al. (2001), while the K_{V0} of Friedrich et al. (2007b) is 2.2% lower than that of Winkler et al. (2001) with the same K'_{V0} . In summary, all recent studies by different methods acquired lower K_{V0} than Xu et al. (1994) and Mao et al. (1994). More importantly, Yoshino et al. (2019) has discussed the reason why Xu et al. (1994) yielded extremely high value of $K_{V0} = 230$ GPa, which is the data correction by Xu et al. (1994) is under high stress from the absence of a pressure medium.

To date, there have also been some experimental studies on the thermal expansion of diaspore at high temperatures (Holland et al., 1996; Grevel et al., 2000; Sugiura et al., 2018). Pawley et al. (1996) calculated the volume thermal expansion coefficient ($\alpha_{V0} = 4.0$ (1) $\times 10^{-5}/\text{K}$) of diaspore up to 533 K based on high-temperature powder XRD data (Pawley et al., 1996). Subsequently, Grevel et al. (2000) recalculated the volume thermal expansion coefficient of diaspore at higher temperatures up to 1073 K using XRD and obtained $\alpha_{V0} = 2.8 \times 10^{-5}/\text{K}$ (Grevel et al., 2000), which is $\sim 30\%$ lower than that of Pawley et al. (1996) (Pawley et al., 1996). Furthermore, Pawley et al. (1996) also calculated the axial thermal expansion coefficients of diaspore and obtained $\alpha_{a0} = 1.6$ (2) $\times 10^{-5}/\text{K}$, $\alpha_{b0} = 1.3$ (2) $\times 10^{-5}/\text{K}$ and $\alpha_{c0} = 1.1$ (2) $\times 10^{-5}/\text{K}$ (Pawley et al., 1996). Recently, Sugiura et al. (2018) reinvestigated the axial thermal expansion of diaspore up to 698 K by single-crystal XRD

and obtained $\alpha_{a0} = 0.903 \times 10^{-5}/\text{K}$, $\alpha_{b0} = 0.828 \times 10^{-5}/\text{K}$ and $\alpha_{c0} = 0.770 \times 10^{-5}/\text{K}$ (Sugiura et al., 2018), which are $\sim 44\%$, ~ 36 and $\sim 30\%$ lower, respectively, than the results of Pawley et al. (1996). Thus, there is still great controversy regarding the thermal expansion coefficients of diaspore, which needs to be further investigated.

In this study, we investigated the thermoelasticity and stability of diaspore by *in situ* synchronous XRD and Raman spectroscopy methods at high pressure and high temperature. By fitting the present P - V and T - V XRD data, we obtained the thermoelastic parameters of diaspore at high pressures/temperatures. Furthermore, the P - T stability of diaspore in this experimental P - T range was determined using our high P - T XRD data and Raman spectral data. Finally, combined with the previous results, we discussed the P - T phase diagram and stability of diaspore and its great influence on water migration in the cold subduction zone.

SAMPLE AND EXPERIMENTS

Sample

A natural, colorless and transparent diaspore sample with good crystal morphology was used in this study. As shown in **Supplementary Table S1**, the chemical composition of the diaspore sample was estimated as $\text{Al}_{1.002}\text{Fe}_{0.003}\text{OOH}$ based on the results of electron microprobe analysis (EMPA) using a JXA-8230 electron microprobe in Chang'An University with an accelerating voltage of 15 kV, a beam current of 20 nA, and a beam diameter of 5 μm .

Experiments

We conducted single-crystal XRD experiments up to 700 K and 13.42 GPa, powder XRD experiments up to 713 K under ambient pressure.

A short symmetrical diamond-anvil cell (DAC) and BX90-type external-heating DAC (EHDAC) (Kantor et al., 2012) were selected for ambient temperature and high pressure (up to 13.42 GPa) and high temperature and high pressure (up to 10.9 GPa and 700 K) single crystal XRD experiments, respectively. In the above two XRD experiments, the rhenium gasket, neon pressure medium, and gold pressure calibration material were selected. The sample size and thickness of diaspore are $70 \times 80 \mu\text{m}^2$ and 22 μm , respectively.

In the *in situ* ambient pressure and high temperature (up to 713 K with 30 K temperature interval) powder XRD experiment, a Merrill-Bassett type DAC and the T301 gasket were used. The sample size and thickness of diaspore in the sample chamber are $120 \times 100 \mu\text{m}^2$, and $\sim 110 \mu\text{m}$, respectively.

In addition, the short symmetrical DAC and T301 gasket were used for the high-pressure Raman spectroscopy experiment. The maximum experimental pressure was ~ 24.4 GPa, and the Raman spectrum collected from 100 cm^{-1} – 1200 cm^{-1} . In all experiments, the pressure fluctuation range was not more than 0.1 GPa, and the temperature fluctuation range was not more than 1 K before and after each spectrum collection.

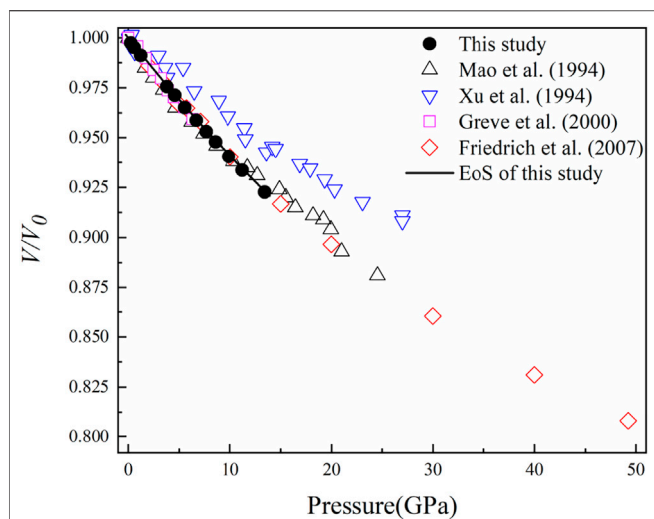


FIGURE 2 | Volume compression (V/V_0) of diaspore at high pressure and room temperature. The black solid circles represent the data points measured in this experiment, and the black lines were obtained by BM3 EoS-fitting with K'_{V0} unfixed. The black hollow triangles represent the data points of Mao et al. (1994), the blue hollow triangles represent the data points of Xu et al. (1994), the purple hollow squares represent the data points of Grevel et al. (2000), and the red hollow diamonds represent the data points of Friedrich et al. (2007a, and 2007b).

The ambient temperature and high pressure single-crystal XRD experiment was conducted at 13-BMD station, GSECARS, APS, while the high temperature and high pressure single-crystal XRD experiment was conducted at 13-BMC station, GSECARS, APS. LaB_6 powder was used as the diffraction standard at both 13-BMD and 13-BMC stations (Fan et al., 2010; Zhang et al., 2017; Huang et al., 2020; Xu et al., 2020). However, the high-temperature and ambient-pressure powder XRD experiment was carried out at station 4W2, Beijing Synchrotron Radiation Station (BSRF), and calibrated by CeO_2 powder diffraction spectrum. Room-temperature and high-pressure Raman spectroscopy experiments were carried out at the Center for High Pressure Science and Technology Advanced Research. Details of the single crystal XRD experimental setup and cell assembly were described in Fan et al. (2010) and the powder XRD experiment were described in Huang et al. (2020) and Xu et al. (2020).

RESULTS

P-V Equation of State

The unit-cell parameters of diaspore up to 13.42 GPa were refined by APEX3 software from single-crystal XRD, as shown in **Supplementary Table S2** and **Figure 2**. The XRD patterns of diaspore showed that no phase transition occurred throughout the whole pressure range in this study (**Supplementary Figure S1**).

Furthermore, the *P-V* data (**Supplementary Table S2**) were fitted using the third-order Birch-Murnaghan EoS as follows:

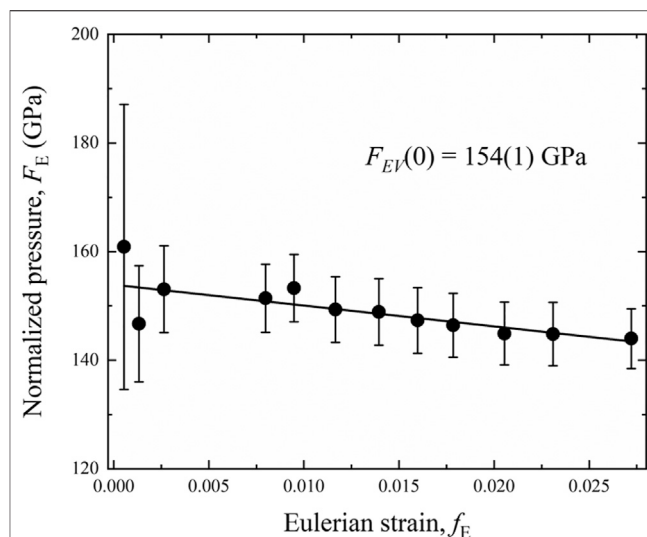


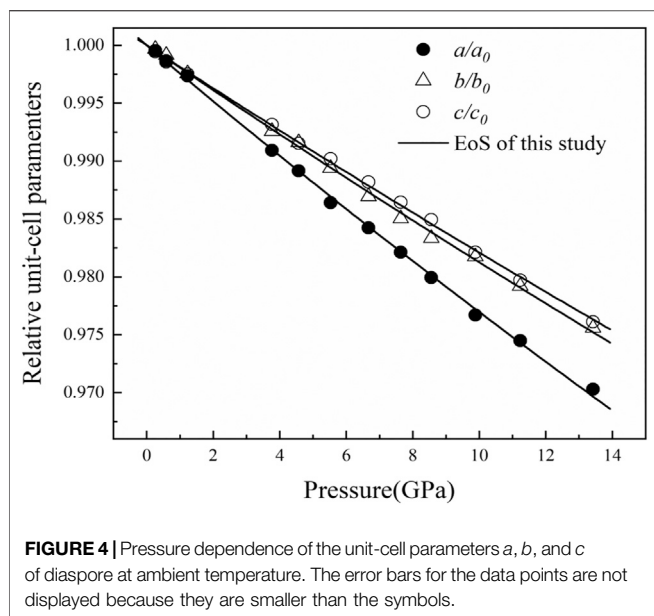
FIGURE 3 | Volume Eulerian strain-normalized pressure (F_E-f_E) plot. The solid line is the linear fit to the data.

$$P = (3/2) K_{V0} [(V_0/V)^{7/3} - (V_0/V)^{5/3}] \times [1 + (3/4)(K'_{V0} - 4) [(V_0/V)^{2/3} - 1]] \quad (1)$$

Where V_0 , K_{V0} , and K'_{V0} are the unit-cell volume, isothermal bulk modulus, and its pressure derivative at zero pressure, respectively. With all parameters unfixed during fitting, we yielded $V_0 = 118.04$ (3) \AA^3 , $K_{V0} = 153$ (2) GPa, and $K'_{V0} = 2.5$ (3) for diaspore. With fixed $K'_{V0} = 4$, the fitting results yielded $V_0 = 118.15$ (4) \AA^3 and $K_{V0} = 143$ (1) GPa.

Figure 2 shows pressure-induced volume compression (V/V_0) of diaspore in this study and previous studies (Mao et al., 1994; Xu et al., 1994; Grevel et al., 2000; and Friedrich et al., 2007a and 2007b). The relationship between the Eulerian definition of finite strain f_E ($f_E = [(V_0/V)^{2/3} - 1]/2$) and “normalized stress” F_E ($F_E = P/3f_E(1 + 2f_E)^{5/2}$) is shown in **Figure 3** (Angel, 2000). The weighted linear fit of the data points yielded the intercept value of $F_E(0) = 154$ (1) GPa, which is consistent with the isothermal bulk modulus obtained by the third-order Birch-Murnaghan EoS ($K_{V0} = 153$ (2) GPa). Moreover, it is clear from **Figure 3** that the data points lie on an inclined straight line with a relatively large negative slope, thus indicating that $K'_{V0} = 2.5$ and the third-order Birch-Murnaghan EoS are reasonable descriptions of the *P-V* data in this study.

The unit-cell parameters of the *a*-, *b*- and *c*-axes as a function of pressure are summarized in **Supplementary Table S2** and plotted in **Figure 4**. By fitting a “linearized” third-order Birch-Murnaghan EoS and following the procedure implemented in the EoSFit7c program (Angel, 2000), we can obtain the axial-EoS parameters $K_{a0} = 137$ (5) GPa, $K_{b0} = 169$ (7), and $K_{c0} = 178$ (6) GPa for the *a*-, *b*- and *c*-axes with fixed $K'_0 = 4$, respectively. Then, the axial compressibilities (with $\beta = \frac{1}{3K_0}$, where K_0 is the axial bulk modulus under ambient conditions and β is the compressibility) of diaspore were found to be $\beta_a = 0.00243$ GPa^{-1} , $\beta_b = 0.00197$ GPa^{-1} and $\beta_c = 0.00187$ GPa^{-1} for the *a*-,



b - and c -axes, respectively. The ratio among the lattice compressibility parameters, $\beta_a:\beta_b:\beta_c = 1.30:1.05:1.00$, shows that diaspore has a weak axial compressional anisotropy.

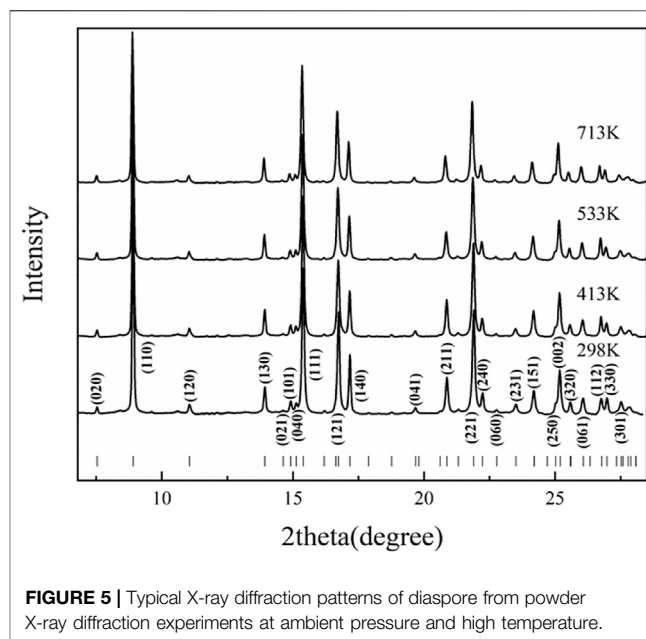
Thermal Expansion

High-temperature synchrotron powder XRD experiments were conducted up to 713 K at ambient pressure. **Figure 5** shows some typical full XRD patterns at high temperatures for diaspore. From **Figure 5**, we can find that as the temperature increased, all the peaks shifted continuously toward lower 2θ , but the overall pattern did not change; hence, the high-temperature XRD patterns of diaspore showed that no phase transformation occurred at high temperatures up to 713 K. **Supplementary Figures S2A–D** shows the typical Le Bail profile fitting results of the XRD profiles at 298, 413, 533 and 713 K. The full spectrum fitting results of unit-cell parameters and volumes (a , b , c , and V) of the Le Bail profile at each temperature are also shown in **Supplementary Table S3**.

Figure 6 shows the variations of a/a_0 , b/b_0 , c/c_0 and V/V_0 with the temperature for diaspore in this study and previous studies. In general, a/a_0 , b/b_0 , c/c_0 and V/V_0 correlate continuously with temperature. As the temperature increases from 297 to 713 K, a , b and c increase by 0.3%, 0.26 and 0.25%, respectively, and volume increases by 0.79%. We used Fei's thermal expansion equation (Fei, 1995) to fit our high-temperature XRD data:

$$V_T = V_0 \exp\left(\alpha_0 (T - T_{\text{ref}}) + (1/2) \alpha_1 (T^2 - T_{\text{ref}}^2) - \alpha_2 \left((1/T) - (1/T_{\text{ref}})\right)\right) \quad (2)$$

Where V_T represents the unit-cell volume at high temperatures and ambient pressure, V_0 represents the unit-cell volume at ambient conditions, and T_{ref} is the reference temperature. α_0 , α_1 and α_2 are the three parameters used to describe the relationship between the thermal expansion coefficient and the temperature in the form of $\alpha_T = \alpha_0 + \alpha_1 T + \alpha_2 T^{-2}$. Since our



experimental temperature range was limited, we fixed α_1 and α_2 as 0 in the fitting. The volumetric and axial thermal expansion coefficients under ambient conditions are $\alpha_V = 2.7 (2) \times 10^{-5} \text{ K}^{-1}$ and $\alpha_a = 1.13 (9) \times 10^{-5} \text{ K}^{-1}$, $\alpha_b = 0.77 (5) \times 10^{-5} \text{ K}^{-1}$, and $\alpha_c = 0.85 (9) \times 10^{-5} \text{ K}^{-1}$. Furthermore, from **Figure 7**, the axial thermal expansion coefficients of diaspore along the b -axis and c -axis are comparable, while the thermal expansion coefficient along the a -axis is the smallest at 300–600 K but is the largest above 600 K. Therefore, diaspore has slightly anisotropy of thermal expansion. Moreover, the single-crystal XRD experiments of diaspore under high P - T conditions show that diaspore can exist stably at conditions of up to 700 K and 10.9 GPa.

Raman Spectroscopy

The high-pressure Raman spectroscopy experiment was conducted up to ~ 24.4 GPa. To study the lattice vibration modes of Al-O-Al and AlO_6 polyhedrons, Raman spectra were collected during the experiment ranging from 150 to 1300 cm^{-1} . There are a total of 11 peaks corresponding to five vibration modes: ν_1 -a rotation of two edge shared AlO_6 , ν_2 -Al-O-Al symmetric stretching, ν_3 -Al-O-Al deformation, ν_4 -Al-O-Al bending, and ν_5 -OH bending (Ruan et al., 2001; Juan-Farfán et al., 2011). The nine peaks with wave numbers less than 1000 cm^{-1} are lattice vibration modes (ν_1 , ν_2 , ν_3 , and ν_4), which mainly include the rotational vibration of AlO_6 and the stretching, bending and deformation vibration of Al-O-Al (Ruan et al., 2001; Juan-Farfán et al., 2011). The remaining two peaks are the OH bending vibration mode (ν_5), whose wave numbers are 1050.3 and 1189.9 cm^{-1} (Delattre et al., 2012). **Figure 8** shows that with increasing pressure, the Raman peak moves toward the high wave number direction, and the intensity increases. **Figure 9** shows that the wave number of each peak increases linearly with increasing pressure. However, the absence of Raman peaks with

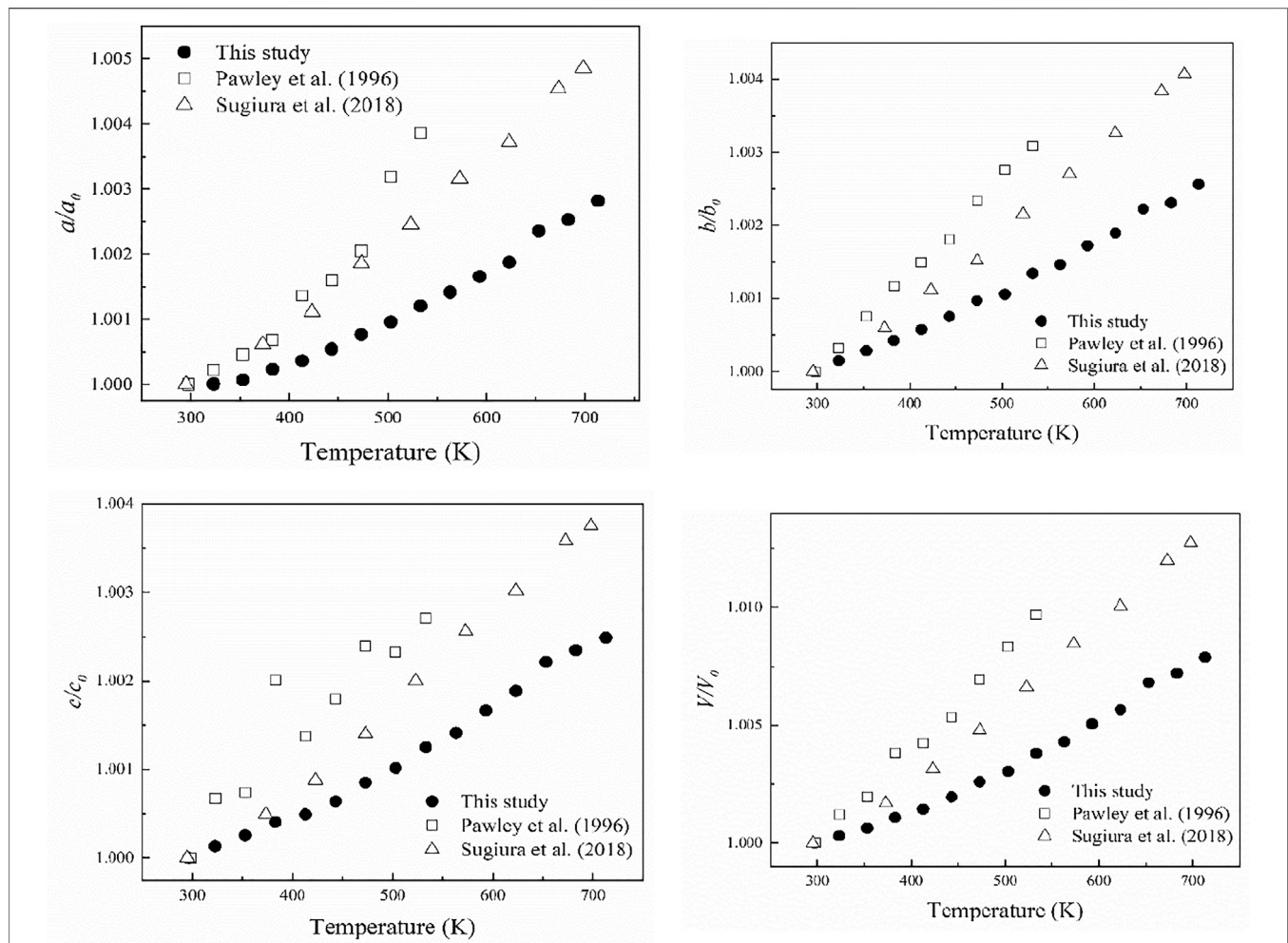


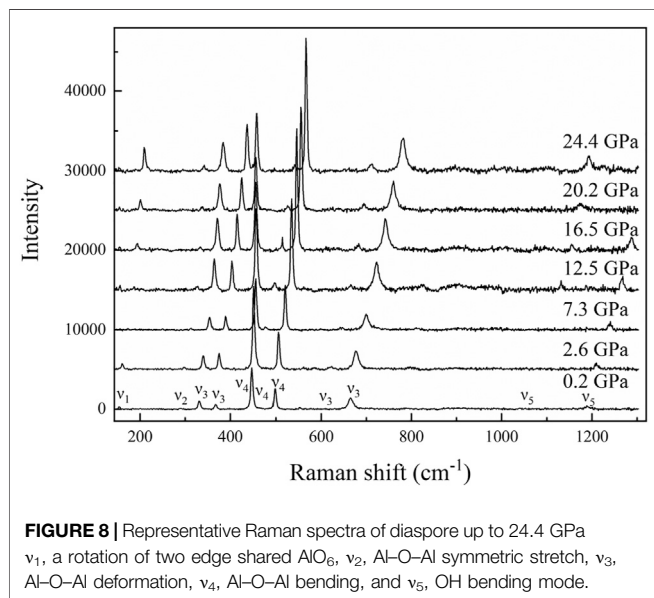
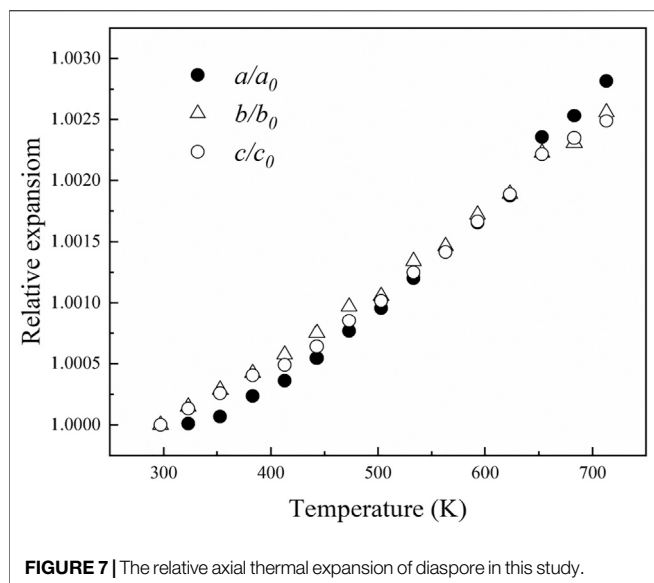
FIGURE 6 | The change of unit-cell parameters and unit-cell volume with increasing temperature. The black solid circles represent the data points of this study, the hollow squares represent the data points of Pawley et al. (1996) and hollow triangles represent the data points of Sugiura et al. (2018).

wave numbers of 154.3 and 1050.3 cm^{-1} is due to the weak peak intensity under high pressures. The missing Raman peak with a wave number of 1189.9 cm^{-1} at high pressures is mainly due to the peak moving toward the high wave number, which exceeds the wave number range in this study. **Table 2** summarizes the Raman spectra of diaspore in this and previous studies at high pressures, showing that the pressure derivative ($d\omega/dP$) of the Raman shift of diaspore is in the range of 0.33–6 $\text{cm}^{-1}/\text{GPa}$, and the Grüneisen parameter ($\gamma = (d\omega/dP) \times K_{V0}/\omega_0$, where ω_0 is the wave number at zero pressure) is in the range of 0.11–2.27.

Juan-Farfán et al. (2011) obtained 22 Raman peaks in the range of 150–1300 cm^{-1} by theoretical calculation. However, only 13 Raman peaks were observed in the same wave number range in experiments (Ruan et al., 2001; Juan-Farfán et al., 2011) because the other peaks were too weak to be observed in the experiments (Ruan et al., 2001; Juan-Farfán et al., 2011). Compared with the experimental result of Juan-Farfán et al. (2011), this study has three extra peaks (448.6, 611.3, and 1189.9 cm^{-1}) and one missing peak (793 cm^{-1}). Compared with the experimental

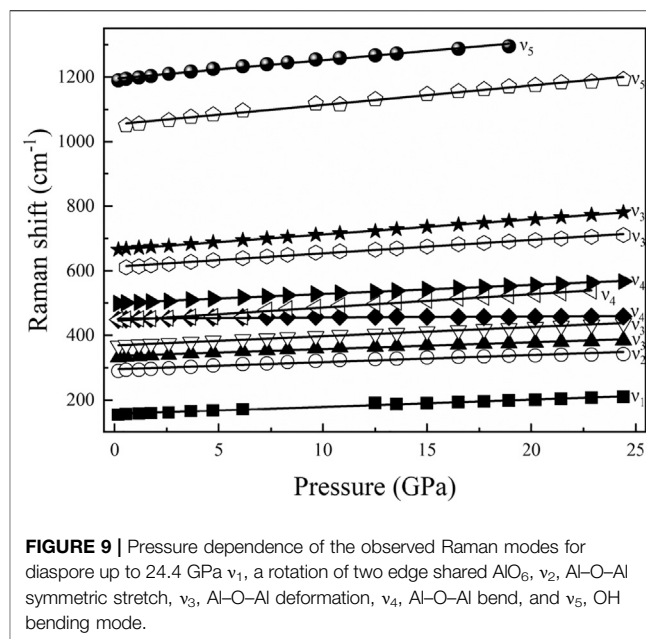
result of Ruan et al. (2001), this study has one extra peak (154.3 cm^{-1}) and two missing peaks (381 and 790 cm^{-1}). The cause of this phenomenon is unknown. However, except for these different peaks, our experimental results are basically consistent with those of previous experiments (**Table 2**) (Greene et al., 1994; Ruan et al., 2001; Juan-Farfán et al., 2011; Delattre et al., 2012).

Based on the experimental results of the Raman spectra, the $d\omega/dP$ and isothermal Grüneisen parameters are calculated in this study (**Table 2**). The value range of $d\omega/dP$ was 0.91–4.94 $\text{cm}^{-1}/\text{GPa}$ by theoretical calculation and 0.33–6 $\text{cm}^{-1}/\text{GPa}$ according to experiments (Juan-Farfán et al., 2011). The range of experimental results is wider than that of the theoretical calculation. Compared with the experimental results of Juan-Farfán et al. (2011), this study shows that the value of $d\omega/dP$ of ν_5 is greater than that of the other vibration modes (ν_1, ν_2, ν_3 and ν_4). Because ν_5 corresponds to the vibration mode of OH bending with increasing pressure, the vibration of OH bending is easier, resulting in a larger $d\omega/dP$ value. Except for the difference



in v_5 value, our experimental results are basically consistent with the experiment of Juan-Farfán et al. (2011).

The value range of the Grüneisen parameter is 0.32–1.59 by theoretical calculation and 0.11–2.27 by experiment. The experimental results show a wider range than the theoretical results. The value of the Grüneisen parameter obtained by this experiment at 1050.3 cm^{-1} is 0.88, while the value of the Grüneisen parameter obtained by the experiment of Juan-Farfán et al. (2011) is 0.3 at 1048 cm^{-1} , which is 66% lower than that in this study. Except for the abnormal value of the Grüneisen parameter at $1050.3/1048 \text{ cm}^{-1}$, the difference between the Grüneisen parameter in this study and that in previous studies is less than 25%. Therefore, the isothermal Grüneisen parameters of the Raman peaks obtained by this study are basically consistent with previous studies.



In conclusion, our high-pressure Raman spectroscopy is consistent with previous results and shows that there is no phase transition of diaspore at room temperature and high pressures up to 24.4 GPa.

DISCUSSION

P-*V* Equation of State

To date, the *P*-*V* EoS of diaspore has been investigated extensively with various experimental techniques. Of these investigations, Xu et al. (1994), Mao et al. (1994), and Friedrich et al. (2007a, and 2007b) used high-pressure XRD methods to study the *P*-*V* EoS of diaspore. **Table 1** summarizes the bulk moduli and their pressure derivatives for diaspore determined with various experimental techniques.

As shown in **Table 1**, the bulk modulus and its pressure derivative of the diaspore obtained in this study are $K_{V0} = 153$ (2) GPa and $K'_{V0} = 2.5$ (3), respectively. If K'_{V0} is set to 4, $K_{V0} = 143$ (1) GPa. The K_{V0} values from the literature exhibit discrepancies with each other, ranging from 121.2 to 227 GPa. Xu et al. (1994) reported a significantly higher value (227 GPa) by DAC with no pressure medium. Subsequently, Mao et al. (1994) obtained $K_{V0} = 168$ (2) GPa and $K'_{V0} = 3$ (1) for diaspore using methanol-ethanol (4:1) pressure medium. However, their maximum experimental pressure reached 24.54 GPa, which exceeded the hydrostatic pressure limit (~ 11 GPa) of the methanol-ethanol (4:1) pressure medium. Thus, the results of Xu et al. (1994) and Mao et al. (1994) should be affected by the nonhydrostatic pressure condition. Later, Friedrich et al. (2007b) reinvestigated the *P*-*V* EoS of diaspore using DAC with two different pressure mediums (methanol-ethanol (4:1) and helium) and obtained $K_{V0} = 150$ (3) GPa and 151 (2) GPa with fixed $K'_{V0} = 4$. The obtained K_{V0} value (143 (1) GPa) in this study with fixed

TABLE 2 | Mode shifts and isothermal Grüneisen parameters of diaspore.

Band assignment	This study			Juan-Farfán et al. (2011)						Ruan et al. (2001)
	Experimental			Experimental			Theoretical			Experimental
	ω_0 (cm ⁻¹)	$d\omega/dP$ (cm ⁻¹ /GPa)	isothermal Grüneisen parameters	ω_0 (cm ⁻¹)	$d\omega/dP$ (cm ⁻¹ /GPa)	isothermal Grüneisen parameters	ω_0 (cm ⁻¹)	$d\omega/dP$ (cm ⁻¹ /GPa)	isothermal Grüneisen parameters	ω_0 (cm ⁻¹)
ν_1	154.3 (1)	2.29 (6)	2.27 (8)	154	1.9	1.91	158	1.67	1.59	—
	—	—	—	—	—	—	182	1.01	0.83	—
ν_2	290 (2)	2.2 (1)	1.16 (6)	288	2.8	1.46	273	2.35	1.29	287
	—	—	—	—	—	—	277	2.36	1.28	—
ν_3	331.5 (1)	2.11 (7)	0.97 (5)	331	2.0	0.91	327	2.63	1.21	329
	—	—	—	—	—	—	357	1.88	0.79	—
ν_3	367.7 (2)	2.84 (2)	1.18 (2)	368	2.6	1.06	362	2.25	0.93	364
	—	—	—	—	—	—	374	1.89	0.76	381
ν_4	447.65 (3)	0.33 (5)	0.11 (2)	448	0.4	0.13	426	0.91	0.32	436
ν_4	448.6 (2)	4.1 (1)	1.40 (6)	—	—	—	433	3.79	1.31	446
ν_4	498.36 (4)	2.81 (2)	0.86 (2)	499	2.7	0.81	480	2.6	0.81	495
	—	—	—	—	—	—	524	2.86	0.82	—
	—	—	—	—	—	—	546	2.25	0.62	—
	—	—	—	—	—	—	562	2.9	0.77	—
	—	—	—	—	—	—	592	4.02	1.02	—
ν_3	611.3 (6)	4.15 (6)	1.04 (3)	—	—	—	631	4.8	1.14	609
ν_3	665.6 (1)	4.70 (1)	1.08 (2)	666	4.3	0.97	636	4.94	1.17	664
	—	—	—	793	2.6	0.49	754	3.46	0.69	790
ν_5	1050.3 (7)	6.0 (1)	0.88 (3)	1048	2.1	0.3	—	—	—	1045
	—	—	—	—	—	—	1092	4.43	0.61	—
	—	—	—	—	—	—	1097	4.42	0.6	—
ν_5	1189.9 (6)	5.7 (2)	0.73 (3)	—	—	—	—	—	—	1186
	—	—	—	—	—	—	1222	4.51	0.55	—
	—	—	—	—	—	—	1227	4.45	0.54	—
	—	—	—	—	—	—	2895	-19.73	-1.02	—
	—	—	—	—	—	—	2918	-18.53	-0.95	2936

ν_1 , a rotation of two edge shared AlO_6 ; ν_2 , Al–O–Al symmetric stretch; ν_3 , Al–O–Al deformation; ν_4 , Al–O–Al bend; and ν_5 , OH bending mode.

$\gamma = (d\omega/dP) \times K_{V0}/\omega_0$, where ω_0 is the wave number at zero pressure.

—, Not observed.

$K'_{V0} = 4$ is slightly smaller than the results (150 (3) GPa and 151 (2) GPa) of Friedrich et al. (2007a, and 2007b) within their uncertainties.

Obviously, as shown in **Figure 2**, the data points of Mao et al. (1994) are consistent with our data points under pressures less than 12.0 GPa. Therefore, we refitted the P - V data of Mao et al. (1994) at pressures within ~ 11.7 GPa and obtained $K_{V0} = 140$ (3) GPa with fixed $K'_{V0} = 4$, which is consistent with the result of this study ($K_{V0} = 143$ (1) GPa) within their uncertainties. Moreover, the obtained K_{V0} value in this study is also very consistent with the results of previous ultrasonic interferometry ($K_{V0} = 145.3$ (4) GPa) and Brillouin light scattering studies ($K_{V0} = 146$ (1) GPa) (**Table 1**) (Haussuhl, 1993; Xu et al., 1994; Grevel et al., 2000; Jiang et al., 2008).

In summary, we infer that the reasonable ranges of the bulk modulus and its pressure derivative of the diaspore should be 140–153 GPa and 2.4–4.5, respectively.

The axial compressibilities of diaspore obtained in this study are $K_{a0}: K_{b0}: K_{c0} = 1.00:1.23:1.30$ ($\beta_a: \beta_b: \beta_c = 1.30:1.05:1.00$), which shows slight axial compression anisotropy. Friedrich et al. (2007a) also obtained the axial compressibilities of diaspore with $K_{a0}: K_{b0}: K_{c0} = 1.00:1.73:1.76$ ($\beta_a: \beta_b: \beta_c = 1.77: 1.02:1.00$) up to

50 GPa with a helium pressure medium. The axial compressibilities of this study are consistent with the axial compression trend of Friedrich et al. (2007a). Both studies show that the c -axis is the least compressible, followed by the b -axis and a -axis, because the Al–Al and O–O bonds are almost parallel to the c -axis, which makes the c -axis the hardest axis. Although there is no bond parallel to the b -axis, the angle between all bonds and the b -axis is 20° – 30° , while the angle between all bonds and the a -axis is greater than 65° , which makes the a -axis the easiest to compress (Li et al., 2008). Furthermore, the compression of the a -axis in the Friedrich et al. (2007a) experiment is much easier than that in this study. We infer that this is probably due to the different pressure ranges between these two studies. Because the O–H bond is almost parallel to the a -axis, the distance between O and H decreases more with increasing pressure, resulting in a greater axial compressibility of the a -axis (Friedrich et al., 2007a). Compared with the compression of the a -axis with increasing pressure, the compression of the b -axis and c -axis are much smaller. The probable reason is that the compression of the a -axis is mainly hydrogen bonding compression, while the compression of the b -axis and c -axis is due to the rotation of the O1–Al–O2 octahedral

TABLE 3 | Comparison of isobaric thermal expansion of diaspore.

Samples	P (GPa)	T (K)	α_V ($10^{-5}/K$) at 300 K	α_a ($10^{-5}/K$) at 300 K	α_b ($10^{-5}/K$) at 300 K	α_c ($10^{-5}/K$) at 300 K	Methods	References
AlO(OH)	0.0001	533	4.0 (1)	1.6 (2)	1.3 (2)	1.1 (2)	PC-XRD ^a	Pawley et al. (1996)
AlO(OH)	7	1073	2.8	—	—	—	XRD	Grevel et al. (2000)
AlO(OH)	0.0001	698	3.0 ^b	0.903	0.828	0.770	SC-XRD ^c	Sugiura et al. (2018)
Al _{1.002} Fe _{0.003} OOH	0.0001	713	2.7 (2)	1.13 (9)	0.77 (5)	0.85 (9)	PC-XRD ^a	This study

—, No data.

^aPowder X-ray diffraction.

^bThe result by recalculating data of Sugiura et al. (2018).

^cSingle-crystal X-ray diffraction.

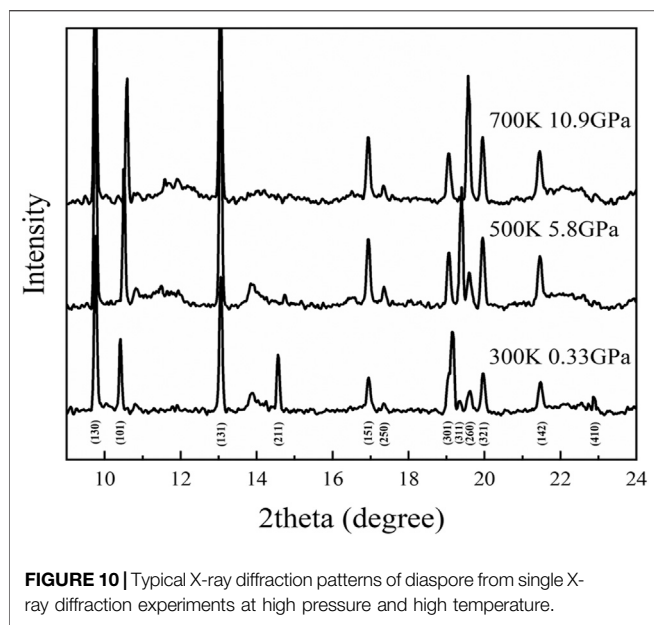
axis angle and the shortening of Al-Al and O-O bonds (Friedrich et al., 2007a; Li et al., 2010), respectively. Although the compressibility of diaspore obtained by Mao et al. (1994) (K_{a0} : K_{b0} : $K_{c0} = 1.00:2.45:2.40$, $\beta_a:\beta_b:\beta_c = 2.45:1:1.01$) shows that the a -axis is the easiest to compress and the b -axis instead of the c -axis is the most difficult to compress, the b -axis is only slightly more difficult to compress than the c -axis. The b -axis and c -axis compression in previous studies are consistent with the results of this study within the uncertainty. Therefore, the obtained axial compressibility in this study should be reliable.

Thermal Expansion

The obtained volume thermal expansion coefficient of diaspore in this study is $\alpha_V = 2.7 (2) \times 10^{-5} K^{-1}$. **Table 3** summarizes the thermal expansion coefficient of diaspore obtained in this study and previous studies. As shown in **Table 3**, Pawley et al. (1996) obtained a volume thermal expansion coefficient of $4.0 (1) \times 10^{-5}/K$ through the powder XRD method at a maximum temperature of 533 K. However, using the same method, Grevel et al. (2000) obtained a volume thermal expansion coefficient of $2.8 \times 10^{-5}/K$ at P - T conditions up to 7 GPa and 1073 K, which is 30% smaller than the result obtained by Pawley et al. (1996). Subsequently, Sugiura et al. (2018) used the single-crystal XRD method to obtain the axial thermal expansion coefficient at the maximum temperature of 698 K but did not give the volume thermal expansion coefficient. The recalculated volume thermal expansion coefficient is $3.0 \times 10^{-5}/K$ by fitting the data of Sugiura et al. (2018) with Fei's thermal expansion equation, which is 25% lower than the result obtained by Pawley et al. (1996).

The obtained volume thermal expansion coefficient in this study ($2.7(2) \times 10^{-5}/K$) is consistent with the results of Sugiura et al. (2018) ($3.0 \times 10^{-5}/K$) and Grevel et al. (2000) ($2.8 \times 10^{-5}/K$) within their uncertainties. Compared with the results of other studies, the volume thermal expansion coefficient obtained by Pawley et al. (1996) is abnormally larger. As shown in **Figure 6**, the experimental results of Pawley et al. (1996) showed a poor relationship between V/V_0 and pressure; in particular, the experimental data points at 110°C significantly deviated from the trend line. Therefore, the volume thermal expansion coefficient obtained by Pawley et al. (1996) was relatively inaccurate. Thus, the volume thermal expansion value of diaspore at 300 K is in the range of 2.7 – $3.0 \times 10^{-5}/K$.

The axial thermal expansion ratios at 300 K obtained in this study, by Pawley et al. (1996), and by Sugiura et al. (2018) are α_a : α_b : $\alpha_c = 1.47:1:1.10$, $1.45:1.18:1$, and $1.17:1.07:1$, respectively, which shows a slight axial thermal expansion anisotropy, mainly due to the different bond distances of Al-O1 and Al-O2 in diaspore. With increasing temperature, the thermal expansion rates of Al-O1 and Al-O2 are not consistent, resulting in the distortion of the AlO₆ octahedron instead of the regular octahedron (Sugiura et al., 2018). This study is consistent with previous studies and shows that the thermal expansion along the a -axis is the largest. According to analyses of Sugiura et al. (2018), the volume thermal expansion of diaspore is larger than that of the AlO₆ octahedron. The excess expansion comes from the expansion of the hydrogen bond channel formed by O2...O1, which is basically parallel to the a -axis. Thus, the axial thermal expansion along the a -axis is greater than that along the b - and c -axes. However, the axial thermal expansion ratio (1.17:1.07:1) among the a -axis, b -axis and c -axis obtained by Sugiura et al. (2018) is slightly lower than that of Pawley et al. (1996) (1.45:1.18:1). Sugiura et al. (2018) considered the main reasons for the difference to be the relatively narrow (298–533 K) temperature range and relatively large unit-cell parameter error of Pawley et al. (1996). Moreover, the temperature range of this study (300–713 K) is similar to that of Sugiura et al. (2018) (300–698 K), and the errors of unit-cell parameters in this study are also relatively small. However, contrary to the results of previous studies, the thermal expansion of the b -axis is slightly less than that of the c -axis in this study. Considering that the thermal expansion along the b -axis and c -axis are similar, we infer that our diaspore sample contains 0.3 mol% Fe, which is different from previous studies. The small amount of Fe may cause a slight change in axial thermal expansion, resulting in the thermal expansion of the b -axis being less than that of the c -axis. In addition, **Figure 6** shows that the axial thermal expansions of Sugiura et al. (2018) are larger than those of this study; however, the axial thermal expansion coefficients of the a -axis and c -axis given by Sugiura et al. (2018) are smaller than those of this study (**Table 3**). The main reason for this difference may be the different fitting methods between these two studies. Thus, we refitted the high-temperature XRD data of Sugiura et al. (2018) using Fei's thermal expansion equation and obtained $\alpha_a = 1.2 \times 10^{-5}/K$, $\alpha_b = 1.0 \times 10^{-5}/K$, and $\alpha_c = 1.0 \times 10^{-5}/K$, which is close to

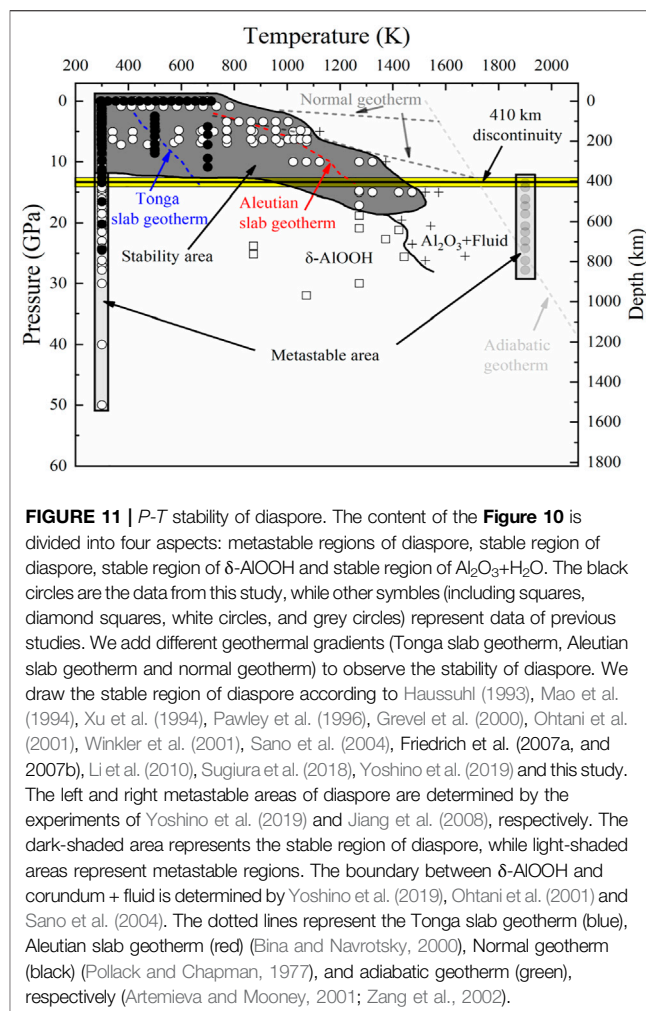


the findings of this study ($\alpha_a = 1.13 \times 10^{-5}/\text{K}$, $\alpha_b = 0.77 \times 10^{-5}/\text{K}$ and $\alpha_c = 0.85 \times 10^{-5}/\text{K}$).

***P-T* Phase Diagram of Diaspore and its Stability Under High *P-T* Conditions**

Water is one of the main volatile components in the Earth's interior and can significantly affect the physical and chemical properties of the main minerals in the deep Earth (Bindi et al., 2020; Brovarone et al., 2020; Doucet et al., 2020; Pieczka et al., 2020; Thompson et al., 2020; Yang et al., 2020). Subducted slabs bring water into the deep Earth, which has a profound influence on the geodynamics of the Earth's interior, such as earthquakes and the formation of island arc magma (Zheng et al., 2016; Zheng and Zhao, 2017; Zheng, 2019; Lempart et al., 2020). Since hydrous minerals are believed to exist in subduction plates and subduct into the mantle together with slab components, the *P-T* stability field of hydrous minerals under high *P-T* conditions is vital for the proposed transportation of water into the deep Earth (Chen et al., 2020; Thompson et al., 2020). Moreover, slab geotherms strongly affect the depth at which hydrous minerals dehydrated in subducting slabs, and thus affect water transport in the deep Earth. For example, under the *P-T* conditions of cold subduction, especially ultracold subduction, hydrous minerals can survive under greater depth in cold subducting slabs, which can transport a large amount of water into the middle and lower part of the upper mantle, even into the transition zone and lower mantle, thus exerting a profound influence on the geological processes of the deep Earth (Wunder et al., 1993a; Pawley, 1994; Holland et al., 1996; Ono, 1999).

Diaspore is an accessory mineral in a metabauxite (metabauxite make up ~11% of continental sedimentary rocks) (Theye et al., 1997; Gao et al., 1998), we roughly speculated that the content of diaspore in the subduction zone is no more than 0.11 vol%. Diaspore is an important hydrous mineral in subduction zones and the high *P-T* stability of diaspore has been investigated widely.



The experimental results of Yoshino et al. (2019) indicated that the dehydration temperature of diaspore increases monotonically from 1123 to 1523 K with increasing pressure from 5 to 15 GPa, while in the experiments of Grevel et al. (2000) diaspore was stable at ~1073 K under 7 GPa. **Figure 11** shows the stability region of diaspore at high *P-T* conditions (Ohtani et al., 2001; Sano et al., 2004; Holland and Powell, 2011; Yoshino et al., 2019). Under normal subduction zone geothermal gradient conditions (Pollack and Chapman, 1977; Artemieva and Mooney, 2001; Zang et al., 2002), diaspore breaks down into corundum and fluid above ~180 km (Wunder et al., 1993b; Pawley et al., 1996; Feenstra and Wunder, 2002; Yoshino et al., 2019). However, in the case of hot subduction conditions, such as the Aleutian subduction zone, diaspore will be transformed into $\delta\text{-AlOOH}$ at 1273 K and 20.9 GPa (Suzuki et al., 2000; Vanpeteghem et al., 2002; Yoshino et al., 2019), while under ultracold subduction conditions, such as the Tonga subduction zone, diaspore can be stabilized to at least 12.5 GPa (Friedrich et al., 2007a; Duan et al., 2018; Yoshino et al., 2019).

Furthermore, the density profile of diaspore was also modeled using its thermal EoS parameters and then compared with other major hydrous minerals (epidote, lawsonite and antigorite) and the

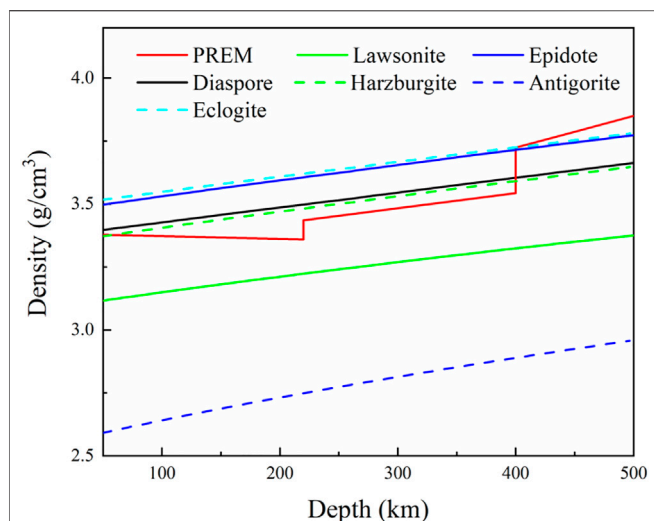


FIGURE 12 | Modeled density profiles of diaspore and other hydrous minerals (Lawsonite (Ballaran and Angel, 2003), Antigorite (Yang et al., 2014), Epidote (Li et al., 2021) and rocks (Harzburgite and Eclogite (Ye et al., 2021)) to ~500 km along the Tonga slab geotherm, and compared with that of the PREM model (Dziewonski and Anderson, 1981).

PREM model (Figure 12). As shown in Figure 12, the density profile of diaspore is ~8 and ~24% higher than lawsonite and antigorite, respectively, but ~3% lower than epidote. The density profile of diaspore is ~4% higher than that of the PREM model above a depth of 410 km. Although diaspore content is low in subducting slab (no more than 0.11 vol%), it might contribute to subduction (Li et al., 2021). However, below a depth of 410 km, the density profile of diaspore is ~5% less than that of the PREM model; thus, diaspore may stagnate along the plate at the top of the mantle transition zone.

Our high P - T experiment indicates that diaspore is metastable up to ~10.9 GPa and 700 K (Figures 10, 11). Combined with the density profile of diaspore (Figure 12), the density of diaspore, eclogite (40% garnet + 55% omphacite + 5% epidote) and harzburgite (74% olivine + 21% orthopyroxene + 3% clinopyroxene + 2% spinel) are higher than ambient mantle (PREM model). Furthermore, the density of diaspore is slightly higher than that of harzburgite but lower than that of eclogite. However, in view of the density of diaspore is higher than ambient mantle (PREM model), diaspore still can subduct together with subduction slabs. To sum up, we believe that diaspore could contribute to slab subduction and bring water into the Earth's interior (at depth approximately 390 km under cold subduction conditions based on existing experimental data) (Ye et al., 2021). Moreover, diaspore dehydrates and releases free H_2O when the subducted slab is heated by the surrounding mantle to a higher temperature. The released H_2O may potentially affect the geochemical behavior of the upper mantle (Gruetznier et al., 2018).

CONCLUSION

The P - V and T - V relationships and P - T stability of diaspore were investigated using *in situ* synchrotron-based single-crystal XRD

and Raman spectroscopy methods up to 713 K and 24.4 GPa in this study. There was no phase transition in the maximum P - T conditions in this study. We fitted unit-cell volume and unit-cell parameter data with third-order Birch–Murnaghan EoS and obtained $V_0 = 118.15$ (4) \AA^3 , $a_0 = 4.3988$ (9) \AA , $b_0 = 9.421$ (2) \AA , $c_0 = 2.8474$ (4) \AA , $K_{V0} = 153$ (1) GPa, $K_{a0} = 137$ (5) GPa, $K_{b0} = 169$ (7) GPa and $K_{c0} = 178$ (6) GPa for diaspore. In addition, using Fei's thermal expansion equation, we obtained the thermal expansion coefficients $\alpha_V = 2.7$ (2) $\times 10^{-5}$ K^{-1} , $\alpha_a = 1.13$ (9) $\times 10^{-5}$ K^{-1} , $\alpha_b = 0.77$ (5) $\times 10^{-5}$ K^{-1} , and $\alpha_c = 0.85$ (9) $\times 10^{-5}$ K^{-1} for diaspore. Finally, combining the results in this study with those of previous studies, we plotted the P - T phase diagram of diaspore and concluded that diaspore can subduct to a depth of ~390 km under cold subduction conditions (temperature gradient <5 K/km) based on existing experimental data.

DATA AVAILABILITY STATEMENT

The original contributions presented in the study are included in the article/Supplementary Material, further inquiries can be directed to the corresponding authors.

AUTHOR CONTRIBUTIONS

Conceptualization and methodology, DF and WZ; investigation, JX and SH; sample source, DL; experimental analysis, DF, WZ, JX, and SH; writing—original draft preparation, SH; writing—review and editing, DF, WZ, MM, SH, JX, ZY, YK, BL, WC, and FC; plotting, SH; software, SH and JX. All authors have read and agreed to the published version of the manuscript.

FUNDING

This work was supported by National Natural Science Foundation of China (Grant Nos. U2032118, 42172048, 41802043, and 41674089), the Youth Innovation Promotion Association CAS (DF, 2018434), the Chinese Academy of Sciences “Light of West China” Program (2017, 2019), the Science and Technology Foundation of Guizhou Province (QKHJC-ZK(2021)ZD042), the Innovation and Entrepreneurship Funding of High-Level Overseas Talents of Guizhou Province (DF, (2019) 10), the Science and Technology Project of Jilin Provincial Department of Education (JJKH20200632KJ), and the Science and Technology Foundation of Changchun Institute of Technology (320210019).

ACKNOWLEDGMENTS

We acknowledge Sergey N. Tkachev for the gas loading assistance. The experimental works were conducted at the GeoSoilEnviroCARS (Sector 13), Advanced Photon Source (APS), and Argonne National Laboratory, the High Pressure Experiment Station (4W2), Beijing Synchrotron Radiation

Facility (BSRF), and the Center for High Pressure Science & Technology Advanced Research (HPSTAR). We would like to thank the two anonymous reviewers for their thorough and helpful comments, which help to improve the quality of this manuscript.

REFERENCES

- Angel, R. J. (2000). Equations of State. *Rev. Mineralogy Geochem.* 41 (1), 35–59. doi:10.2138/rmg.2000.41.2
- Artemieva, I. M., and Mooney, W. D. (2001). Thermal Thickness and Evolution of Precambrian Lithosphere: A Global Study. *J. Geophys. Res.* 106 (B8), 16387–16414. doi:10.1029/2000jb900439
- Ballaran, T. B., and Angel, R. J. (2003). Equation of State and High-Pressure Phase Transitions in Lawsonite. *ejm* 15 (2), 241–246. doi:10.1127/0935-1221/2003/0015-0241
- Bina, C. R., and Navrotsky, A. (2000). Possible Presence of High-Pressure Ice in Cold Subducting Slabs. *Nature* 408 (6814), 844–847. doi:10.1038/35048555
- Bindi, L., Bendeliani, A., Bobrov, A., Matrosova, E., and Irifune, T. (2020). Incorporation of Mg in Phase Egg, AlSiO₃OH: Toward A New Polymorph of Phase H, MgSiH₂O₄, A Carrier of Water in the Deep Mantle. *Am. Mineral.* 105 (1), 132–135. doi:10.2138/am-2020-7204
- Brovarone, A. V., Butch, C. J., Ciappa, A., Cleaves, H. J., Elmaleh, A., Faccenda, M., et al. (2020). Let There Be Water: How Hydration/dehydration Reactions Accompany Key Earth and Life Processes#. *Am. Mineral.* 105 (8), 1152–1160. doi:10.2138/am-2020-7380
- Chen, H., Leinenweber, K., Prakapenka, V., Kunz, M., Bechtel, H. A., Liu, Z., et al. (2020). Phase Transformation of Hydrous Ringwoodite to the Lower-Mantle Phases and the Formation of Dense Hydrous Silica. *Am. Mineral.* 105 (9), 1342–1348. doi:10.2138/am-2020-7261
- Delattre, S., Balan, E., Lazzeri, M., Blanchard, M., Guillaumet, M., Beyssac, O., et al. (2012). Experimental and Theoretical Study of the Vibrational Properties of Diaspore (α -AlOOH). *Phys. Chem. Minerals* 39 (2), 93–102. doi:10.1007/s00269-011-0464-x
- Doucet, L. S., Xu, Y., Klaessens, D., Hui, H., Ionov, D. A., and Mattielli, N. (2020). Decoupled Water and Iron Enrichments in the Cratonic Mantle: A Study on Peridotite Xenoliths from Tok, SE Siberian Craton. *Am. Mineral.* 105 (6), 803–819. doi:10.2138/am-2020-7316
- Duan, Y., Sun, N., Wang, S., Li, X., Guo, X., Ni, H., et al. (2018). Phase Stability and Thermal Equation of State of δ -AlOOH: Implication for Water Transportation to the Deep Lower Mantle. *Earth Planet. Sci. Lett.* 494, 92–98. doi:10.1016/j.epsl.2018.05.003
- Dziewonski, A. M., and Anderson, D. L. (1981). Preliminary Reference Earth Model. *Phys. Earth Planet. Interiors* 25 (4), 297–356. doi:10.1016/0031-9201(81)90046-7
- Ewing, F. J. (1935). The Crystal Structure of Diaspore. *J. Chem. Phys.* 3 (4), 203–207. doi:10.1063/1.1749634
- Fan, D., Zhou, W., Wei, S., Liu, Y., Ma, M., and Xie, H. (2010). A Simple External Resistance Heating diamond Anvil Cell and its Application for Synchrotron Radiation X-ray Diffraction. *Rev. Scientific Instr.* 81 (5), 053903. doi:10.1063/1.3430069
- Feenstra, A., and Wunder, B. (2002). Dehydration of Diasporite to Corundite in Nature and experiment. *Geol.* 30 (2), 119–122. doi:10.1130/0091-7613(2002)030<0119:Dotdci>2.0.Co;2
- Fei, J. C. H. (1995). “A Bird’s Eye View of Policy Evolution in Taiwan an Introductory Essay,” in *Mineral Physics & Crystallography*. Editor T. J. Ahrens, 29–51. doi:10.1142/9789814261487_0002
- Friedrich, A., Haussühl, E., Boehler, R., Morgenroth, W., Juarez-Arellano, E. A., and Winkler, B. (2007a). Single-crystal Structure Refinement of Diaspore at 50 GPa. *Am. Mineral.* 92 (10), 1640–1644. doi:10.2138/am.2007.2549
- Friedrich, A., Wilson, D. J., Haussühl, E., Winkler, B., Morgenroth, W., Refson, K., et al. (2007b). High-pressure Properties of Diaspore, AlO(OH). *Phys. Chem. Minerals* 34 (3), 145–157. doi:10.1007/s00269-006-0135-5
- Gao, S., Zhang, B. R., Jin, Z. M., Kern, H., Luo, T. C., and Zhao, Z. D. (1998). How Mafic Is the Lower continental Crust? (Vol 161, Pg 101, 1998). *Earth Planet. Sci. Lett.* 161 (1–2), 101–117. doi:10.1016/S0012-821X(98)00140-X
- Greene, R. G., Luo, H., and Ruoff, A. L. (1994). High Pressure Raman and EDXD Study of Diaspore. *AIP Conf. Proc.* 309, 1535–1538. doi:10.1063/1.46375

SUPPLEMENTARY MATERIAL

The Supplementary Material for this article can be found online at: <https://www.frontiersin.org/articles/10.3389/feart.2021.752566/full#supplementary-material>

- Grevel, K.-D., Burchard, M., Fasshauer, D. W., and Peun, T. (2000). Pressure-volume-temperature Behavior of Diaspore and Corundum: An In Situ X-ray Diffraction Study Comparing Different Pressure media. *J. Geophys. Res.* 105 (B12), 27877–27887. doi:10.1029/2000jb900323
- Grützner, T., Klemme, S., Rohrbach, A., Gervasoni, F., and Berndt, J. (2018). The Effect of Fluorine on the Stability of Wadsleyite: Implications for the Nature and Depths of the Transition Zone in the Earth’s Mantle. *Earth Planet. Sci. Lett.* 482, 236–244. doi:10.1016/j.epsl.2017.11.011
- Haussühl, S. (1993). Thermoelastic Properties of Beryl, Topaz, Diaspore, Sanidine and Periclae. *Z. Kristallogr* 204, 67–76. doi:10.1524/zkri.1993.204.Part-1.67
- Hebert, L. B., and Montési, L. G. J. (2013). Hydration Adjacent to a Deeply Subducting Slab: The Roles of Nominally Anhydrous Minerals and Migrating Fluids. *J. Geophys. Res. Solid Earth* 118 (11), 5753–5770. doi:10.1002/2013jb010497
- Hill, R. J. (1979). Crystal Structure Refinement and Electron Density Distribution in Diaspore. *Phys. Chem. Minerals* 5 (2), 179–200. doi:10.1007/bf00307552
- Holland, T. J. B., and Powell, R. (2011). An Improved and Extended Internally Consistent Thermodynamic Dataset for Phases of Petrological Interest, Involving a New Equation of State for Solids. *J. Metamorph. Geol.* 29 (3), 333–383. doi:10.1111/j.1525-1314.2010.00923.x
- Holland, T. J. B., Redfern, S. A. T., and Pawley, A. R. (1996). Volume Behavior of Hydrous Minerals at High Pressure and Temperature; II, Compressibilities of Lawsonite, Zoisite, Clinzoisite, and Epidote. *Am. Mineral.* 81 (3–4), 341–348. doi:10.2138/am-1996-3-408
- Huang, S., Xu, J., Chen, C., Li, B., Ye, Z., Chen, W., et al. (2020). Topaz, A Potential Volatile-Carrier in Cold Subduction Zone: Constraint from Synchrotron X-Ray Diffraction and Raman Spectroscopy at High Temperature and High Pressure. *Minerals* 10 (9), 780. doi:10.3390/min10090780
- Hwang, G. C., Hwang, H., Bang, Y., Choi, J., Park, Y., Jeon, T.-Y., et al. (2021). A Role for Subducted Albite in the Water Cycle and Alkalinity of Subduction Fluids. *Nat. Commun.* 12 (1), 1155. doi:10.1038/s41467-021-21419-6
- Jiang, F., Majzlan, J., Speziale, S., He, D., and Duffy, T. S. (2008). Single-crystal Elasticity of Diaspore, AlOOH, to 12GPa by Brillouin Scattering. *Phys. Earth Planet. Interiors* 170 (3–4), 221–228. doi:10.1016/j.pepi.2008.05.011
- Juan-Farfan, R. E., Bayarjargal, L., Winkler, B., Haussühl, E., Avalos-Borja, M., Refson, K., et al. (2011). Pressure Dependence of the Lattice Dynamics of Diaspore, α -AlO(OH), from Raman Spectroscopy and Density Functional Perturbation Theory. *Phys. Chem. Minerals* 38 (9), 693–700. doi:10.1007/s00269-011-0442-3
- Kakizawa, S., Inoue, T., Nakano, H., Kuroda, M., Sakamoto, N., and Yurimoto, H. (2018). Stability of Al-Bearing Superhydrous Phase B at the Mantle Transition Zone and the Uppermost Lower Mantle. *Am. Mineral.* 103 (8), 1221–1227. doi:10.2138/am-2018-6499
- Kantor, I., Prakapenka, V., Kantor, A., Dera, P., Kurnosov, A., Sinogeikin, S., et al. (2012). BX90: A New Diamond Anvil Cell Design for X-ray Diffraction and Optical Measurements. *Rev. Scientific Instr.* 83 (12), 125102. doi:10.1063/1.4768541
- Lempart, M., Derkowski, A., Strączek, T., and Kapusta, C. (2020). Systematics of H₂ and H₂O Evolved from Chlorites During Oxidative Dehydrogenation. *Am. Mineral.* 105 (6), 932–944. doi:10.2138/am-2020-7326
- Li, B., Xu, J., Zhang, D., Ye, Z., Huang, S., Fan, D., et al. (2021). Thermoelasticity and Stability of Natural Epidote at High Pressure and High Temperature: Implications for Water Transport During Cold Slab Subduction. *Geosci. Front.* 12, 921–928. doi:10.1016/j.gsf.2020.05.022
- Li, M., Li, L. X., Yang, W. M., Zhang, P. F., and Zou, G. T. (2008). The Behavior of Diaspore Under High Pressure and High Temperature. *Chin. J. Phys.* 22 (3), 333–336. doi:10.11858/gywlb.2008.03.020
- Li, M., Snoussi, K., Li, L., Wang, H., Yang, W., and Gao, C. (2010). Diaspore Crystal Structure and Compressibility at High Pressures and High Temperature. *Appl. Phys. Lett.* 96 (26), 261902. doi:10.1063/1.3457919
- Liu, D., Hirner, S. M., Smyth, J. R., Zhang, J., Shi, X., Wang, X., et al. (2021). Crystal Chemistry and High-Temperature Vibrational Spectra of Humite and Norbergite: Fluorine and Titanium in Humite-Group Minerals. *Am. Mineral.* 106 (7), 1153–1162. doi:10.2138/am-2021-7538

- Liu, X., Matsukage, K. N., Nishihara, Y., Suzuki, T., and Takahashi, E. (2019). Stability of the Hydrous Phases of Al-Rich Phase D and Al-Rich Phase H in Deep Subducted Oceanic Crust. *Am. Mineral.* 104 (1), 64–72. doi:10.2138/am-2019-6559
- Mao, H.-k., Shu, J., Hu, J., and Hemley, R. J. (1994). High-pressure X-ray Diffraction Study of Diaspore. *Solid State. Commun.* 90 (8), 497–500. doi:10.1016/0038-1098(94)90053-1
- Nakao, A., Iwamori, H., and Nakakuki, T. (2016). Effects of Water Transportation on Subduction Dynamics: Roles of Viscosity and Density Reduction. *Earth Planet. Sci. Lett.* 454, 178–191. doi:10.1016/j.epsl.2016.08.016
- Ohtani, E., Litasov, K., Suzuki, A., and Kondo, T. (2001). Stability Field of New Hydrous Phase, δ -AlOOH, with Implications for Water Transport into the Deep Mantle. *Geophys. Res. Lett.* 28 (20), 3991–3993. doi:10.1029/2001gl013397
- Ono, S. (1999). High Temperature Stability Limit of Phase Egg, AlSiO₃ (OH). *Contrib. Mineralogy Pet.* 137 (1-2), 83–89. doi:10.1007/s004100050583
- Pawley, A. R., Redfern, S. A. T., and Holland, T. J. B. (1996). Volume Behavior of Hydrous Minerals at High Pressure and Temperature; I, Thermal Expansion of Lawsonite, Zoisite, Clinozoisite, and Diaspore. *Am. Mineral.* 81 (3-4), 335–340. doi:10.2138/am-1996-3-407
- Pawley, A. R. (1994). The Pressure and Temperature Stability Limits of Lawsonite: Implications for H₂O Recycling in Subduction Zones. *Contr. Mineral. Petrol.* 118 (1), 99–108. doi:10.1007/bf00310614
- Pieczka, A., Ertl, A., Gołębiewska, B., Jeleń, P., Kotowski, J., Nejbart, K., et al. (2020). Crystal Structure and Raman Spectroscopic Studies of OH Stretching Vibrations in Zn-Rich Fluor-Elbaite. *Am. Mineral.* 105 (11), 1622–1630. doi:10.2138/am-2020-7360
- Pollack, H. N., and Chapman, D. S. (1977). Regional Variation of Heat-Flow, Geotherms, and Lithospheric Thickness. *Tectonophysics* 38 (3-4), 279–296. doi:10.1016/0040-1951(77)90215-3
- Ruan, H. D., Frost, R. L., and Klopogge, J. T. (2001). Comparison of Raman Spectra in Characterizing Gibbsite, Bayerite, Diaspore and Boehmite. *J. Raman Spectrosc.* 32 (9), 745–750. doi:10.1002/jrs.736
- Sano, A., Ohtani, E., Kondo, T., Hirao, N., Sakai, T., Sata, N., et al. (2008). Aluminous Hydrous Mineral δ -AlOOH as a Carrier of Hydrogen into the Core-Mantle Boundary. *Geophys. Res. Lett.* 35 (3), L03303. doi:10.1029/2007gl031718
- Sano, A., Ohtani, E., Kubo, T., and Funakoshi, K.-i. (2004). In Situ X-ray Observation of Decomposition of Hydrous Aluminum Silicate AlSiO₃OH and Aluminum Oxide Hydroxide δ -AlOOH at High Pressure and Temperature. *J. Phys. Chem. Sol.* 65 (8-9), 1547–1554. doi:10.1016/j.jpccs.2003.12.015
- Sugiura, T., Arima, H., Nagai, T., and Sugiyama, K. (2018). Structural Variations Accompanied by Thermal Expansion of Diaspore: In-Situ Single-crystal and Powder X-ray Diffraction Study. *Phys. Chem. Minerals* 45 (10), 1003–1010. doi:10.1007/s00269-018-0981-y
- Suzuki, A., Ohtani, E., and Kamada, T. (2000). A New Hydrous Phase δ -AlOOH Synthesized at 21 GPa and 1000 °C. *Phys. Chem. Minerals* 27 (10), 689–693. doi:10.1007/s002690000120
- Theye, T., Chopin, C., Gravel, K.-D., and Ockenga, E. (1997). The Assemblage Diaspore+quartz in Metamorphic Rocks: A Petrological, Experimental and Thermodynamic Study. *J. Metamorph Geol.* 15 (1), 17–28. doi:10.1111/j.1525-1314.1997.1501050.x
- Thompson, E. C., Davis, A. H., Brauser, N. M., Liu, Z., Prakapenka, V. B., and Campbell, A. J. (2020). Phase Transitions in ϵ -FeOOH at High Pressure and Ambient Temperature. *Am. Mineral.* 105 (12), 1769–1777. doi:10.2138/am-2020-7468
- Tropper, P., and Manning, C. E. (2007). The Solubility of Corundum in H₂O at High Pressure and Temperature and its Implications for Al Mobility in the Deep Crust and Upper Mantle. *Chem. Geology* 240 (1-2), 54–60. doi:10.1016/j.chemgeo.2007.01.012
- Vanpeteghem, C. B., Ohtani, E., and Kondo, T. (2002). Equation of State of the Hydrous Phase δ -AlOOH at Room Temperature up to 22.5 GPa. *Geophys. Res. Lett.* 29 (7), 3. doi:10.1029/2001gl014224
- Wang, R., and Yoshino, T. (2021). Electrical Conductivity of Diaspore, δ -AlOOH and ϵ -FeOOH. *Am. Mineral.* 106 (5), 774–781. doi:10.2138/am-2021-7605
- Winkler, B., Hytha, M., Pickard, C., Milman, V., Warren, M., and Segall, M. (2001). Theoretical Investigation of Bonding in Diaspore. *ejm* 13 (2), 343–349. doi:10.1127/0935-1221/01/0013-0343
- Wunder, B., Medenbach, O., Krause, W., and Schreyer, W. (1993a). Synthesis, Properties and Stability of Al₃Si₂O₇(OH)₃ (Phase Pi), A Hydrous High - Pressure Phase in the System Al₂O₃ - SiO₂ - H₂O (ASH). *ejm* 5 (4), 637–650. doi:10.1127/ejm/5/4/0637
- Wunder, B., Rubie, D. C., Ross, C. R., Medenbach, O., Seifert, F., and Schreyer, W. (1993b). Synthesis, Stability, and Properties of Al₂SiO₄(OH)₂: A Fully Hydrated Analogue of Topaz. *Am. Mineral.* 78 (3-4), 285–297.
- Xu, J.-a., Hu, J., Ming, L.-c., Huang, E., and Xie, H. (1994). The Compression of Diaspore, AlO(OH) at Room Temperature up to 27 GPa. *Geophys. Res. Lett.* 21 (3), 161–164. doi:10.1029/94gl00026
- Xu, J., Fan, D., Zhang, D., Li, B., Zhou, W., and Dera, P. K. (2020). Investigation of the Crystal Structure of a Low Water Content Hydrous Olivine to 29.9 GPa: A High-Pressure Single-crystal X-ray Diffraction Study. *Am. Mineral.* 105 (12), 1857–1865. doi:10.2138/am-2020-7444
- Yang, C., Inoue, T., and Kikegawa, T. (2021). P-V-T Equation of State of Hydrous Phase A up to 10.5 GPa. *Am. Mineral.* 106 (1), 1–6. doi:10.2138/am-2020-7132
- Yang, C., Inoue, T., Yamada, A., Kikegawa, T., and Ando, J.-i. (2014). Equation of State and Phase Transition of Antigorite Under High Pressure and High Temperature. *Phys. Earth Planet. Interiors* 228, 56–62. doi:10.1016/j.pepi.2013.07.008
- Ye, Z., Fan, D., Tang, Q., Xu, J., Zhang, D., and Zhou, W. (2021). Constraining the Density Evolution During Destruction of the Lithospheric Mantle in the Eastern North China Craton. *Gondwana Res.* 91, 18–30. doi:10.1016/j.gr.2020.12.001
- Yoshino, T., Baker, E., and Duffey, K. (2019). Fate of Water in Subducted Hydrous Sediments Deduced from Stability fields of FeOOH and AlOOH up to 20 GPa. *Phys. Earth Planet. Interiors* 294, 106295. doi:10.1016/j.pepi.2019.106295
- Zang, S.-X., Liu, Y.-G., and Ning, J.-Y. (2002). Thermal Structure of Lithosphere in North China. *Chin. J. Geophys.* 45 (1), 51–62. doi:10.1002/cjg2.216
- Zhang, D., Dera, P. K., Eng, P. J., Stubbs, J. E., Zhang, J. S., Prakapenka, V. B., et al. (2017). High Pressure Single Crystal Diffraction at PX2. *JoVE* 119, 9. doi:10.3791/54660
- Zhang, L., Smyth, J. R., Kawazoe, T., Jacobsen, S. D., Niu, J., He, X., et al. (2019). Stability, Composition, and Crystal Structure of Fe-Bearing Phase E in the Transition Zone. *Am. Mineral.* 104 (11), 1620–1624. doi:10.2138/am-2019-6750
- Zheng, Y.-F. (2019). Subduction Zone Geochemistry. *Geosci. Front.* 10 (4), 1223–1254. doi:10.1016/j.gsf.2019.02.003
- Zheng, Y.-F., and Zhao, Z.-F. (2017). Introduction to the Structures and Processes of Subduction Zones. *J. Asian Earth Sci.* 145, 1–15. doi:10.1016/j.jseaes.2017.06.034
- Zheng, Y., Chen, R., Xu, Z., and Zhang, S. (2016). The Transport of Water in Subduction Zones. *Sci. China Earth Sci.* 59 (4), 651–682. doi:10.1007/s11430-015-5258-4

Conflict of Interest: The authors declare that the research was conducted in the absence of any commercial or financial relationships that could be construed as a potential conflict of interest.

Publisher's Note: All claims expressed in this article are solely those of the authors and do not necessarily represent those of their affiliated organizations, or those of the publisher, the editors and the reviewers. Any product that may be evaluated in this article, or claim that may be made by its manufacturer, is not guaranteed or endorsed by the publisher.

Copyright © 2021 Huang, Xu, Liu, Li, Ye, Chen, Kuang, Chi, Fan, Ma and Zhou. This is an open-access article distributed under the terms of the Creative Commons Attribution License (CC BY). The use, distribution or reproduction in other forums is permitted, provided the original author(s) and the copyright owner(s) are credited and that the original publication in this journal is cited, in accordance with accepted academic practice. No use, distribution or reproduction is permitted which does not comply with these terms.